Int. J. Electrochem. Sci., 16 **(2021)** Article Number: 211218, doi: 10.20964/2021.12.05

International Journal of
ELECTROCHEMICAL
SCIENCE
www.electrochemsci.org

The adsorption and inhibition mechanism of 1-Phenyltetrazole-5-thiol for X70 steel corrosion in H_2SO_4 medium

Yanyan Xu[1,2], *Wenwen Xiao*[1,2], *Pengli Ge*[1,2], *Wenguang Zeng*[1,2], *Qingshan Liu*[1,2], *Zhengyuan Gao*[3,*], *Yongbo Yan*[4]

[1] SINOPEC Northwest Company of China Petroleum and Chemical Corporation, Urumqi 830011, China
[2] Key Laboratory of Enhanced Oil Recovery in Carbonate Fractured-vuggy Reservoirs, SINOPEC, Urumqi 830011, China
[3] School of Mechatronics & Vehicle Engineering, Chongqing Jiaotong University, Chongqing, 400074, China
[4] School of Oil and Natural Gas Engineering, Southwest Petroleum University, Chengdu 610500
[*]E-mail: zhengyuangao@cqjtu.edu.cn (Z. Gao); yanyongbo0520@163.com

Received: 5 August 2021 / *Accepted:* 18 September 2021 / *Published:* 10 November 2021

This work aimed to develop a high-efficiency and reliable alternative for conventional and toxic corrosion inhibitor. A novel tetrazole derivative (1-Phenyltetrazole-5-thiol, PTT) that possessed excellent anti-corrosion capacity was exploited for the first time. Based on the traditional electrochemical investigation, morphological observation, and computer modeling, inhibition ability and adsorption type of PTT for X70 steel in 0.5 M H_2SO_4 were varied. The electrochemical results showed that PTT was a mixed organic inhibitor, which could retard charge transfer impedance, and slowed down the corrosion rate of steel. Specifically, the highest inhibition efficiency was 95.1% when the added PTT dose was 2 mM. The adsorption model showed that the PTT film was formed via powerful physicochemical adsorption. As shown in theoretical calculations, the lower ΔE, higher μ values and $E_{binding}$ value of PTT corresponded to supreme adsorption performance, which was also a manifestation of the PTT high-efficiency corrosion inhibition.

Keywords: Corrosion inhibitor, Tetrazole derivative, Steel, Electrochemistry, Theoretical calculation

1. INTRODUCTION

Metal is one of the most indispensable parts in industrial development and is widely used in manufacturing various machinery and equipment, such as heat exchangers, pipelines, and boilers [1-3]. There is no doubt that the application of metal has promoted social progress and economic development

[4-6]. However, metal is easily corroded when it works in various harsh conditions, especially in acidic environments. The corrosive media can diffuse into the inside of metal as the corrosion increases appreciably. Finally, the mechanical and chemical properties of the metal can decrease due to serious corrosion [7, 8]. Obviously, this phenomenon will cause huge economic losses and serious safety accidents.

To slow down metal corrosion, a large number of anti-corrosion strategies have been developed, for example, corrosion inhibitors [9, 10], electrochemical protection [11], coatings [12, 13], and polymetallic doping [14, 15]. In the above technologies, the addition of corrosion inhibitors is one of the most useful anti-corrosion methods, especially in the acidic environment of oil extraction. Conventional corrosion inhibitors can be divided into two categories, namely inorganic corrosion inhibitors and organic corrosion inhibitors. Inorganic corrosion inhibitors can decrease metal corrosion by forming passivation film or precipitation film. These protective films are unreliable because there is no interaction between inorganic corrosion inhibitors and the metal surface. Moreover, a series of inorganic corrosion inhibitors are harmful to humans and the environment, such as chromate, nitrite, and polyphosphate [16, 17]. Hence, they have been banned or replaced by organic corrosion inhibitors [18].

Organic corrosion inhibitors generally contain heteroatoms (N, O, S, P), benzene rings, and double bonds, facilitating the adsorption of organic molecules on the metal surface through physical and/or chemical effects [19, 20]. In addition, compared with inorganic corrosion inhibitors, organic corrosion inhibitors are less harmful to humans and the environment. Therefore, so many corrosion inhibitors were developed by researchers. Qiang et al. investigated the corrosion inhibition of losartan potassium (LP) via traditional electrochemical, in-situ electrochemical methods, weight loss, and theoretical calculation [21]. The results showed that LP could efficiently decrease the corrosion rate of Q235 steel in the HCl medium and the highest anti-corrosion efficiency was 94.0%. Li et al. reported that *brassica oleracea* L extract was an excellent corrosion inhibitor for Q235 steel in two harsh acid environments [22]. Obot et al. found 2-(2-pyridyl) benzimidazole could be eligible as a high-efficiency corrosion inhibitor on API X60 steel, even under turbulent hydrodynamics [23].

1-Phenyltetrazole-5-thiol (PTT) consists of a benzene ring, a nitrogen-containing nitrogen heterocycle, and a mercapto group, all of which help PTT adsorb on the metal surface. The chemical structure of PTT and potential configuration transformation is displayed in Fig. 1.

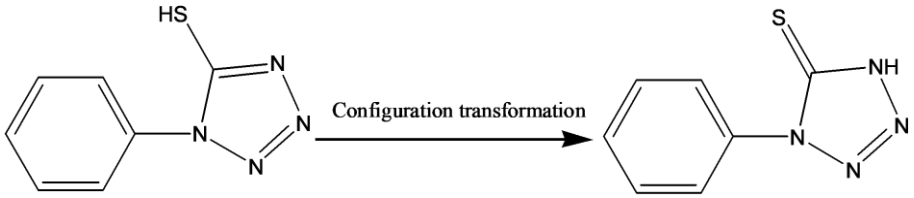

Figure 1. The chemical structure and potential configuration transformation of PTT.

As far as we are aware, no work is getatable focusing on the anti-corrosion of PTT for X70 steel in the H_2SO_4 medium. In this study, the inhibition of PTT for X70 steel corrosion was investigated by conventional electrochemical test and scanning electron microscope (SEM) observation. Meanwhile, Langmuir adsorption and quantum chemical calculation explored the interaction mechanism between

PTT and X70 steel. Finally, this study could offer a new understanding of organic anti-corrosion mechanism and a useful direction for developing novel organic as effective inhibitors in practical application.

2. EXPERIMENTAL

2.1 Materials

X70 steel was widely used in the oil extraction industry and was provided by SINOPEC Northwest Company of China Petroleum and Chemical Corporation. The tested area of the working electrode was 1 × 1 cm^2, and other parts were covered by epoxy resin. 1-Phenyltetrazole-5-thiol (≥ 98%) was purchased from Shanghai Aladdin Biochemical Technology Co., Ltd. and was used without other purification. The test 0.5 M H_2SO_4 (blank solution) solution was obtained by diluting concentrated sulfuric acid (98%). The tested concentrations of PTT were 0.2, 0.5, 1, 2 mM and used a new solution before each experiment.

2.2 Electrochemical tests

The traditional electrochemical tests were executed by a three-electrode system, which contained a working electrode (X70 steel), a reference electrode (saturated calomel electrode), and a counter electrode (2 × 2 cm^2 platinum sheet). To obtain a metastable state, the X70 steel electrode was immersed in the test solution for a period of time. After that, the AC impedance was carried out from 10^5 to 10^{-2} Hz frequency range with a 5 mV sinusoidal disturbance. Potentiodynamic polarization was employed to explore the current density variation of steel surface further. The potential range of the above test was ± 250 mV versus $E_{ocp,}$ and the scanning rate was 1 mV/s. All electrochemical experiments were executed on a thermostat water bath, and the temperature fluctuation was no more than ± 0.5 ℃.

2.3 Surface characterization

In order to observe the variation of the X70 steel surface more directly, the SEM test was employed. The tested samples were polished with emery paper (400-7000 mesh) and then ultrasonic washed with alcohol and acetone to remove oil and impurities. After that, these samples were quickly dried by N_2. The prepared samples were immersed in 0.5 M H_2SO_4 (with and without 2 mM PTT) for 1 h. The whole observation process was executed under the high vacuum condition via SEM (JEOL-JSM-7800F).

2.4 Calculation details

The whole theoretical calculation of PTT in this study was executed by Gaussian 09 W software [24]. Considering that PTT may undergo a configuration transformation in the acid environment, another

structure of PTT was also calculated. Two different molecule structures of PTT were optimized by GGA/B3LYP method (6-311++G(d, p) module) at the DFT level [25]. Then, a battery of parameters were obtained and discussed carefully. The interaction between PTT (two structures) and Fe (110) atoms was explored based on the Forcite module of molecular dynamics method. An emulation cell of 29.8 × 19.4 × 65.2 Å dimension containing 3 layers Fe (110) was established. Moreover, 1 PTT molecule and 300 water molecules were added to the cell. Meanwhile, COMPASS force field and periodic boundary condition were employed in the cell [26, 27]. The simulation time was 100 ps, and the time step was 1 fs under NVT canonical ensemble.

3. RESULTS AND DISCUSSION

3.1 Electrochemical analysis

3.1.1 EIS

As shown in Fig. 2a, the EIS spectra of X70 steel in various PTT concentrations were given. It could be seen that all EIS curves showed an imperfect semicircle, even in a higher PTT concentration. Meanwhile, this phenomenon was also called frequency dispersion.

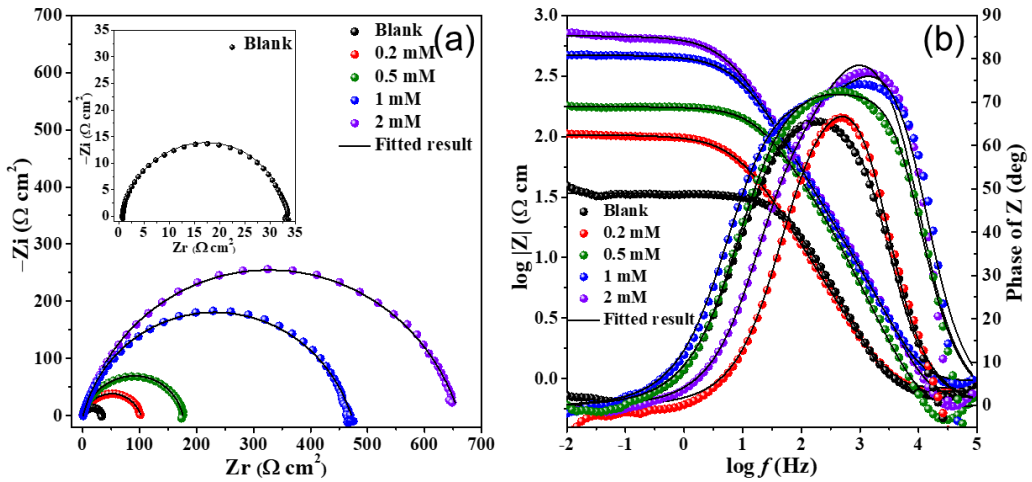

Figure 2. The electrochemical spectra of various PTT concentrations in 0.5 M H_2SO_4 solution at room temperature.

These irregular semicircles were attributed to the different roughness of the X70 steel surface and the non-uniform adsorption of PTT [28, 29]. Compared with the blank EIS curve, the EIS semicircle size became larger when the PTT was presented, and this phenomenon was more prominent with an increase in PTT concentration. This finding meant that the protective film was fabricated by the adsorption of PTT molecules on the metal surface. At the same time, with the increase of PTT concentration, this film became more powerful to resist the attack of corrosive ions. In addition, all EIS

curves showed a similar shape, which indicated that PTT only increased the resistance value of the steel surface but didn't alter the properties of the systematic electrochemical parameters [30, 31].

The corresponding bode modulus and phase angle plots of X70 steel were displayed in Fig. 2b. As we all know, the impedance modulus value of the lowest frequency (10^{-2} Hz) represented the polarization impedance. It was easy to notice that the polarization impedance of X70 steel was increased when PTT presented and continue to augment. Furthermore, the impedance modulus of the highest PTT concentration (2 mM) was about 1.5 orders of magnitude higher than blank. This phenomenon indicated that more PTT molecules formed a stable shield film and thus endowed steel with excellent anti-corrosion ability. Meanwhile, the slope between *log*Z and *logf* was close to −1, implying the traditional capacitive behavior. Therefore, we could infer that the adsorption of PTT on the metal surface was tight and orderly [32].

In order to further quantify the anti-corrosion ability of PTT, the original EIS data were fitted by Zsimpwin, and the corresponding equivalent circuit was shown in Fig. 3.

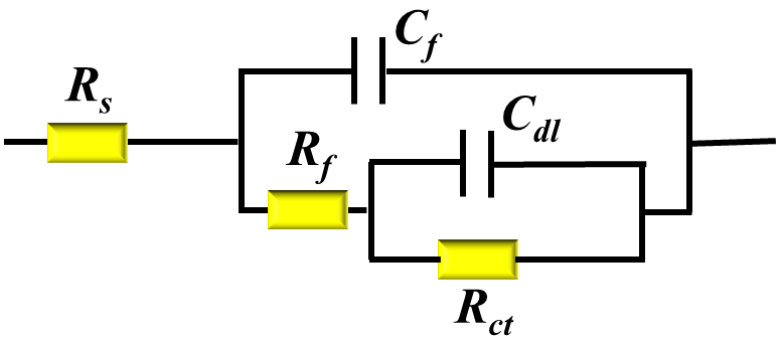

Figure 3. The equivalent circuit for fitting EIS data.

A series of electrochemical parameters, such as solution resistance (R_s), film resistance (R_f), charge-transfer resistance (R_{ct}), polarization resistance (R_p), film capacitance (C_f), and electrical double-layer capacitance (C_{dl}) was obtained and discussed. The C_f and C_{dl} were replaced by CPE_f and CPE_{dl} due to the non-ideal test condition. The value of inhibition ability (η_E) could be calculated by Eq. 1.

$$\eta_E = \frac{R_p - R_{p,0}}{R_p} \times 100\% \quad (1)$$

Here, $R_{p,0}$ stood for polarization resistance without PTT, and R_p was the same resistance with various PTT.

Moreover, the CPE_f and CPE_{dl} were calculated as follows [33].

$$Z_{CPE} = Y_0(2\pi f_{Z_{im-Max}})^{n-1} \quad (2)$$

Where Y_0 presented the modulus, f presented the max frequency of impedance imaginary part, and n was the dispersion coefficient, which related to the flatness of the metal surface.

After original EIS data were fitted, some important parameters were displayed in Table 1. As shown in Table 1, the R_f and R_{ct} values were increased with the advent of PTT, and they keep increasing as the concentration of PTT increased.

Table 1. Impedance parameters of X70 steel in 0.5 M H_2SO_4 with various PTT concentrations at room temperature.

C (mM)	R_s (Ω cm^2)	R_f (Ω cm^2)	R_{ct} (Ω cm^2)	R_p (Ω cm^2)	C_f (μF cm^{-2})	n_1	C_{dl} (μF cm^{-2})	n_2	η (%)
Blank	0.8	5.8	26.7	32.5	75.7	1	128.7	0.82	–
0.2	1.1	7.1	94.4	101.5	56.8	1	107.8	0.74	68.0
0.5	1.5	55.6	120.5	176.1	26.1	1	43.5	0.78	81.5
1	1.7	58.1	412.8	470.9	16.9	1	28.2	0.74	93.1
2	1.6	73.3	587.6	660.9	11.3	1	17.6	0.76	95.1

At the same time, the R_p value also increased from 101.5 (0.2 mM) to 600.9 (2 mM) Ω cm^2, while the impedance of X70 steel in 0.5 M vitriol was 32.5 Ω cm^2. The huge increase in polarization impedance could be explained by that PTT equipped an excellent inhibition film. Quite the opposite, the value of CPE_f in 2 mM was the smallest, only 11.3 μF cm^{-2}, while the blank value of CPE_f was75.7 μF cm^{-2}. This phenomenon could be attributed to replacing H_3O^+ with PTT adsorbed on the metal surface, which reduced the exposed area of metal in acid and thus enhanced metal anti-corrosion ability. Meanwhile, the CPE_{dl} value was decreased from 128.7 to 17.6 μF cm^{-2}. Based on the Helmholtz model, the change in CPE_{dl} was corresponding to the decrease of dielectric constant and the augment of electric double-layer thickness and protected steel area. Finally, the η_E was enhanced and reached 95.1% when the added concentration of PTT was 2mM. In a word, the corrosion of X70 steel in acid was inhibited by the powerful protective film derived from the strong adsorption of PTT on the steel surface.

3.2 Potentiodynamic polarization curves

The polarization curves of X70 steel in various PTT concentrations were given in Fig. 4. Compared with the blank curve, the corrosion potential showed a negative shift trend, which might be related to the replacement of the H_3O^+ by PTT on the metal surface and was also consistent with the above EIS results [34].

In addition, the cathodic curve exhibited a descend trend when PTT was added in the corrosive medium, and descend extent was more distinct with the increase of PTT concentration. Clearly, the appearance of PTT effectively slowed down the cathodic corrosion rate of the steel. However, the shape of the cathodic branch was not affected by the adsorption of PTT, meaning the hydrogen evolution reaction at the cathode wasn't changed [35]. For the anodic curve, a similar descend trend to the cathodic branch was observed when the added PTT concentration was 0.2, 0.5, and 1 mM. But when the concentration of PTT was 2 mM, a platform was noticed from □0.46 V to □0.30 V, showing that enough PTT molecules resisted the desorption phenomenon caused by the increase in polarization potential. This finding also indirectly proved the successful adsorption of PTT molecules on the metal surface.

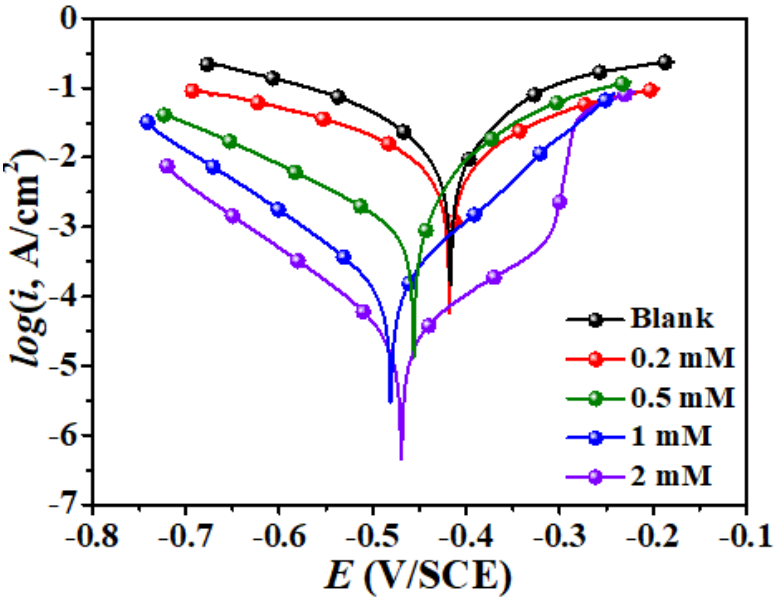

Figure 4. Potentiodynamic polarization curves of PTT for X70 steel in 0.5 M H_2SO_4 medium at room temperature.

Accordingly, a series of important parameters, such as cathodic and anodic Tafel slopes (β_c and β_a), E_{corr}, and i_{corr} were obtained and explored deeply. Moreover, the η_T was also calculated by Eq. 3.

$$\eta_T = \frac{i_{corr,0} - i_{corr}}{i_{corr,0}} \times 100\% \quad (3)$$

Where i_{corr} and $i_{corr,0}$ were current densities of steel that contained and lacked various PTT.

Table 2. Potentiodynamic polarization parameters of X70 steel in 0.5 M H_2SO_4 with various PTT concentrations.

C **(mM)**	E_{corr} **(mV/SCE)**	I_{corr} **(μA cm^{-2})**	β_c **(mV dec^{-1})**	β_a **(mV dec^{-1})**	η **(%)**
Blank	–417	2275	–151	129	–
0.2	–418	794.1	–178	158	65.1
0.5	–456	445.9	–142	105	80.4
1	–481	175.2	–102	121	92.3
2	–469	118.3	–104	90	94.8

As shown in Table 2, the i_{corr} value was declined with the appeared of PTT and continued to reduce when the concentration of PTT increased. Compared with the blank current densities (2275 μA cm^{-2}), the i_{corr} of 2 mM PTT was 118.3 μA cm^{-2}, which was much smaller than blank i_{corr} (at least an order of magnitude). Furthermore, the highest η_T was 94.8%, indicating that the PTT could endow X70 steel incomparable anti-corrosion capacity in 0.5 M H_2SO_4 due to the highly stable PTT organic protective film. In addition, the variation of E_{corr} was no more than 85 mV when compared with blank.

This finding indicated that PTT was a mixed corrosion inhibitor, which could simultaneously suppress steel anodic and cathodic corrosion reactions.

3.3 Corrosion morphology

SEM is one of the most conventional tools to observe the corrosion morphology of metal. Herein, the corrosion morphology of X70 steel that contained and lacked 2 mM PTT was given in Fig. 5. As shown in Fig. 5a, the steel surface was very rough, and some peaks and valleys also appeared due to the serious corrosion.

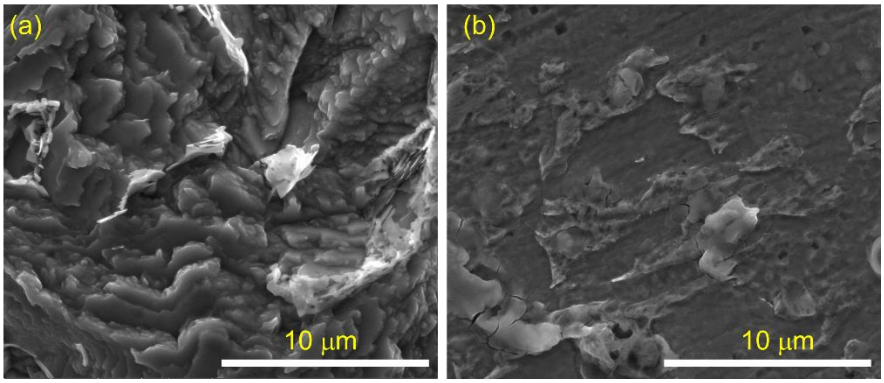

Figure 5. The microtopography of X70 steel after being immersed in 0.5 M H_2SO_4 solution with and without 2 mM PTT at room temperature.

Obviously, bare X70 steel was hard to resist the attack of 0.5 M H_2SO_4 without PTT protection. Fortunately, the morphology of steel with 2 mM PTT protection was smooth, and only a few corrosion products were observed. This finding indicated that a wonderful shield film was formed by the adsorption of PTT and thus resisted the violent attack of the corrosive medium. This result was also consistent with the above EIS and Tafel conclusions.

3.4 Adsorption model

The isothermal adsorption model was one of the most effective methods to explore organic molecules adsorption type. In addition, many different adsorption models were used to investigate the adsorption of inhibitors, such as ElAwady, Fumkin, Langmuir, and Freundlich, Floy-Huggins [36]. After fitted EIS data, we noticed that Langmuir was the most suitable adsorption model to explain the adsorption mechanism of PTT in the above adsorption models. That was to say, PTT molecules possessed impartial probability to adsorb on the steel surface and no interaction between them. Accordingly, some thermodynamic parameters were obtained from the following formulas, such as equilibrium (K_{ads}) and standard adsorption free energy (ΔG^0_{ads}) [37].

$$\frac{C}{\theta} = \frac{1}{K_{ads}} + C \quad (4)$$

$$K_{ads} = \frac{1}{55.5}\exp(-\frac{\Delta G^0_{ads}}{RT}) \quad (5)$$

Where *C* meant the PTT concentration, θ was the Q235 steel surface coverage, *R* represented the molar gas constant, and *T* was the Kelvin temperature.

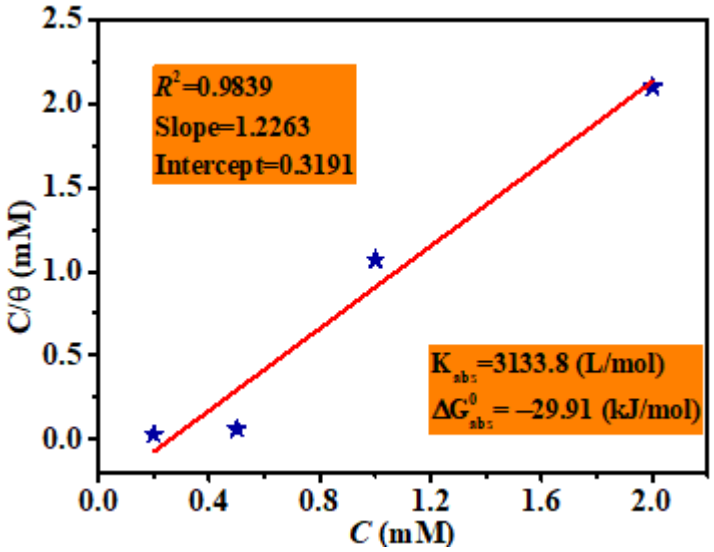

Figure 6. Langmuir adsorption curve and some important thermodynamic parameters of various PTT concentrations.

As shown in Fig. 6, the linear regression coefficient (R^2) was 0.9839 and was infinitely close to 1, implying that the fitted result was dependable. The bigger K_{ads} and smaller ΔG^0_{ads} corresponded to a powerful interaction performance between organic molecules and the metal surface. In addition, the ΔG^0_{ads} value of PTT (−29.91 kJ/mol) was between −20 kJ/mol and −40 kJ/mol, indicating that the adsorption type of PTT in steel was the mixed type (physicochemical adsorption).

3.5 Quantum chemical calculation

Quantum chemical calculation was executed to explore the relationship between structure and reactivity of PTT. Due to the potential configuration transformation of PTT, another structure of PTT was also calculated. Fig. 7 shown the optimized geometry and FMO of PTT. All functional groups were in the same plane for optimized geometry structures, which foreboded that they possessed a smaller steric hindrance. As shown in Figs. 7b and c, the LUMO electron cloud of PTT was located in the benzene ring, tetrazole ring, and hydrosulphonyl. The HOMO electron cloud was similar to LUMO, dispersing on all functional groups of PTT. For PTT after configuration transformation, the intensity and breadth of the FMO electron cloud became weaker, but they were also distributed over the entire PTT. These phenomena manifest that both PTT structures had good adsorption capacity.

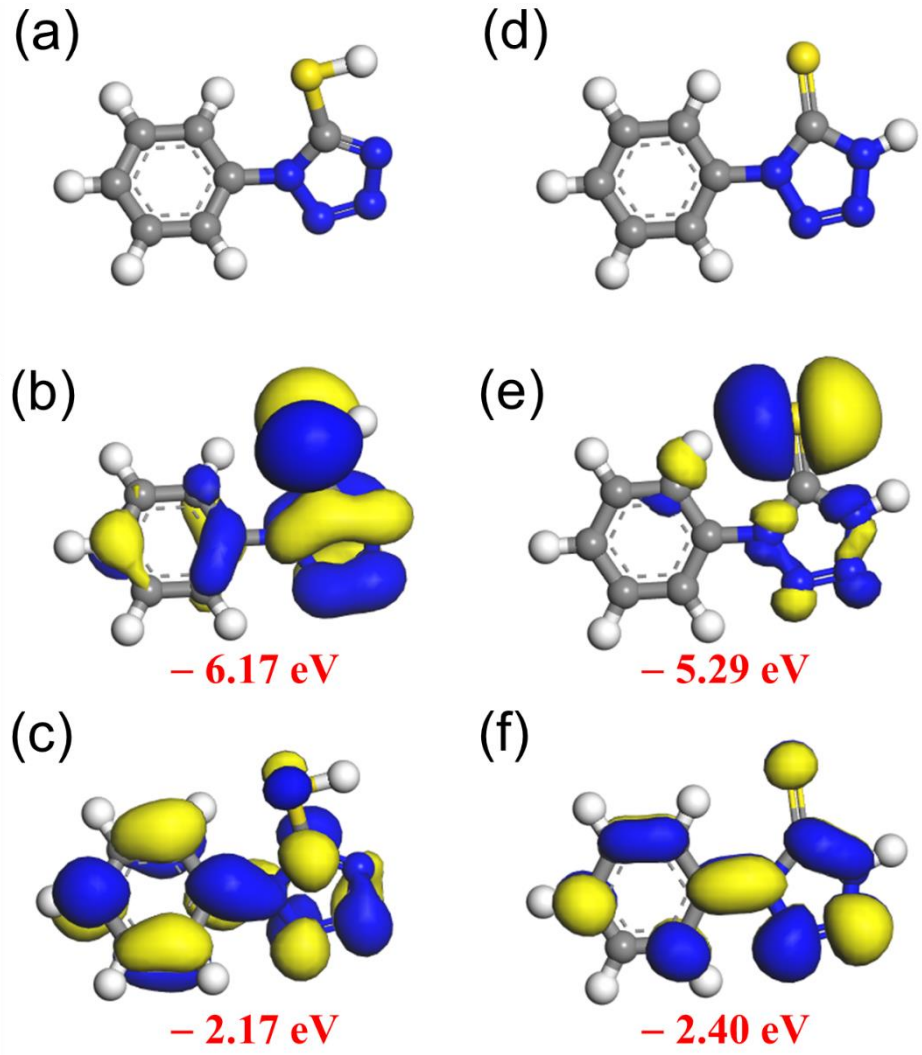

Figure 7. The optimized geometry structure and FMO of PTT molecule before and after configuration transformation.

The value of LUMO and HOMO stood for the obtained electrons and given electrons capacity of a compound, respectively. The lowest LUMO value was related to the highest gained electrons ability, while the highest HOMO value corresponded to the strongest donated performance [38]. Hence, a lower energy gap ($\Delta E = E_{LUMO} - E_{HOMO}$) meant a powerful adsorption performance and thus represented a supreme anti-corrosion efficiency. As given in Fig. 7, ΔE values of both PTT structures were 4.00 and 2.89 eV, respectively, indicating that PTT possessed higher chemical reactivity and was polarizable. Moreover, dipole moment values (μ) of PTT in both structures were 5.51 and 0.76 Debye, respectively, which meant PTT could easily adsorb on the X70 steel owing to dipole-dipole interaction [39]. In a word, PTT could adsorb on the metal surface in parallel and then given steel an excellent anti-corrosion capacity.

3.6 Molecular dynamics simulation

To more intuitively understand the adsorption form of PTT on the X70 steel surface, we performed an MD simulation. There was no doubt that both PTT structures were considered and discussed in MD simulation.

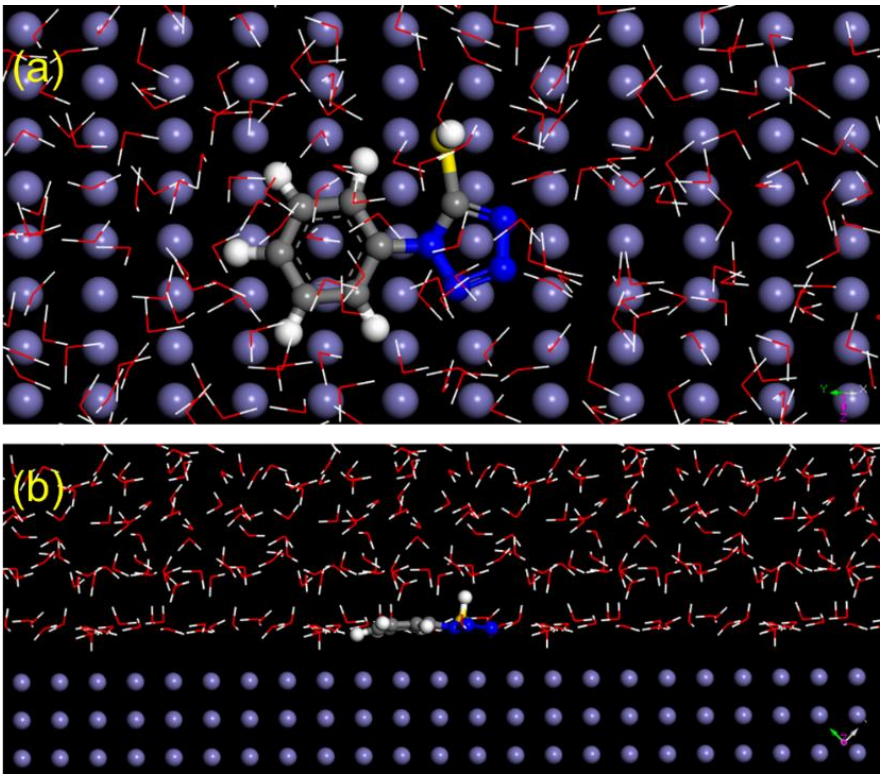

Figure 8. The interface interaction simulation of PTT/Fe (110), (a) top view and (b) side view.

As shown in Fig. 8, PTT could absorb on Fe (110) in parallel via benzene ring, tetrazole ring, and sulfur atom. After PTT finished configuration transformation, the adsorption model was more parallel when compared with the above result. These findings indicated that both PTT structures could adsorb on steel surface in parallel and reduced the contact area between steel and corrosive medium.

Furthermore, parallel adsorption mode was also conducive to the gained and given of electrons between PTT and steel surface and further promoted the formation of coordination bond between PTT and steel surface [40-44]. On the other hand, the $E_{binding}$ values between PTT and steel without and with configuration transformation were 82.3 and 90.1 Kcal/mol, respectively. Compared with reported works, PTT possessed higher $E_{binding}$ values, which was also reliable evidence and direct explanation for PTT supreme corrosion inhibition ability in both structures.

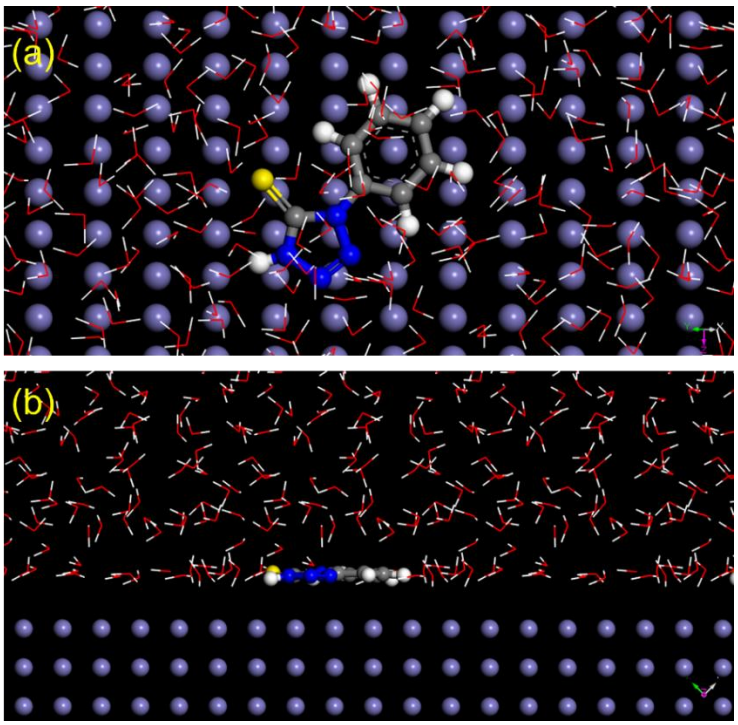

Figure 9. The interface interaction simulation of PTT/Fe (110) after PTT finished configuration transformation, (a) top view and (b) side view.

4. CONCLUSIONS

A series of systematic experiments and theoretical methods examined the anti-corrosion capacity of PTT for X70 steel in 0.5 M H_2SO_4. The following results were given from this work:

1. EIS results showed that PTT possessed excellent anti-corrosion ability for X70 steel in acidic corrosion medium owing to PTT could effectively inhibit the charge transfer on the steel surface. Meanwhile, the η_E enhanced with the increase of PTT concentration, and the highest value reached 95.1%.

2. Based on analysis results of Tafel curves, we found that PTT was a modest organic inhibitor, which could significantly reduce the i_{corr} value of steel surface. Moreover, cathodic and anodic reactions were weakened when PTT appeared and became more obvious with the concentration of PTT increased.

3. Langmuir adsorption indicated that the interface interaction forces between PTT and X70 steel surface were physisorption and chemisorption. SEM results further demonstrated the strong protection ability of PTT film for steel in acid solution.

4. In theoretical calculation, the anti-corrosion mechanism of PTT was revealed at a microcosmic degree. The evenly distributed FMO implied the excellent electronic conversion ability between PTT and Fe (110), further verified by the lower ΔE and higher μ values. The high $E_{binding}$ value meant powerful interaction in PTT/Fe (110) interface and thus corresponding to supreme inhibition performance.

References

1. Y. Qiang, S. Zhang, B. Tan and S. Chen, *Corros. Sci.,* 133 (2018) 6-16.
2. B. Tan, S. Zhang, H. Liu, Y. Guo, Y. Qiang, W. Li, L. Guo, C. Xu and S. Chen, *J. Colloid Interf. Sci.,* 538 (2019) 519-529.
3. A. Singh, K.R. Ansari, D.S. Chauhan, M.A. Quraishi, H. Lgaz and I.-M. Chung, *J. Colloid Interf. Sci.,* 560 (2020) 225-236.
4. M. Ramezanzadeh, M. Asghari, B. Ramezanzadeh and G. Bahlakeh, *Chem. Eng. J.*, 337 (2018) 385-397.
5. M. Ramezanzadeh, B. Ramezanzadeh, M. Mahdavian and G. Bahlakeh, *Carbon* 161 (2020) 231-251.
6. M. Cui, J. Dong, K. Zhou, Y. Fang, J. Pu, H. Zhao, Y. Wang and L Wang, *Int. J. Electrochem. Sci.,* 13(2018) 12010-12023.
7. J. Zhang and H. Li, *Int. J. Electrochem. Sci.*, 15(2020) 4368-4378.
8. J. Zhang and H. Li, *Int. J. Electrochem. Sci.,* 15(2020) 5362-5372.
9. Y. Qiang, H. Li and X. Lan, *J. Mater. Sci. Technol.,* 52 (2020) 63-71.
10. Y. Qiang, S. Zhang, L. Guo, X. Zheng, B. Xiang and S. Chen, *Corros. Sci.*, 119 (2017) 68-78.
11. G. Zhang, L. Wu, A. Tang, Y. Ma, G.-L. Song, D. Zheng, B. Jiang, A. Atrens and F. Pan, *Corros. Sci.,* 139 (2018) 370-382.
12. H. Li, Y. Qiang, W. Zhao and S. Zhang, *Corros. Sci.,* 191 (2021) 109715.
13. W. Wang, H. Wang, J. Zhao, X. Wang, C. Xiong, L. Song, R. Ding, P. Han and W. Li, *Chem. Eng. J.,* 361 (2019) 792-804.
14. B. Jiang, Q. Xiang, A. Atrens, J. Song and F. Pan, *Corros. Sci.*, 126 (2017) 374-380.
15. L. Li, Y. Zhang, J. Lei, J. He, R. Lv, N. Li and F. Pan, *Corros. Sci.,* 85 (2014) 174-182.
16. D.A. Winkler, M. Breedon, P. White, A.E. Hughes, E.D. Sapper and I. Cole, *Corros. Sci.*, 106 (2016) 229-235.
17. H. Li, S. Zhang and Y. Qiang, *J. Mol. Liq.*, 321 (2021) 114450.
18. L. Feng, S. Zhang, Y. Feng, X. Ren, H. Lu, B. Tan and S. Chen, *Chem. Eng. J.*, 394 (2020) 124909.
19. L. Guo, S. Kaya, I.B. Obot, X. Zheng and Y. Qiang, *J. Colloid Interf. Sci.,* 506 (2017) 478-485.
20. L. Guo, S. Zhu, S. Zhang, Q. He and W. Li, *Corros. Sci.,* 87 (2014) 366-375.
21. Y. Qiang, L. Guo, H. Li and X. Lan, *Chem. Eng. J.*, 406 (2021) 126863.
22. H. Li, Y. Qiang, W. Zhao and S. Zhang, *Colloid Surf. A* 616 (2021) 126077.
23. I.B. Onyeachu, I.B. Obot, A.A. Sorour and M.I. Abdul-Rashid, *Corros. Sci.,* 150 (2019) 183-193.
24. B. Tan, J. He, S. Zhang, C. Xu, S. Chen, H. Liu and W. Li, *J Colloid Interf. Sci.,* 585 (2021) 287-301.
25. Y. Qiang, S. Zhang, H. Zhao, B. Tan and L. Wang, *Corros. Sci.,* 161 (2019) 108193.
26. M. Ramezanzadeh, G. Bahlakeh, B. Ramezanzadeh and Z. Sanaei, *J. Ind. Eng. Chem.,* 77 (2019) 323-343.
27. M. Murmu, S.K. Saha, N.C. Murmu and P. Banerjee, *Corros. Sci.,* 146 (2019) 134-151.
28. Z. Zhang, N. Tian, W. Zhang, X. Huang, L. Ruan and L. Wu, *Corros. Sci.,* 111 (2016) 675-689.
29. G. Quartarone, M. Battilana, L. Bonaldo and T. Tortato, *Corros. Sci.*, 50(12) (2008) 3467-3474.
30. P. Mourya, P. Singh, R.B. Rastogi and M.M. Singh, *Appl. Surf. Sci.,* 380 (2016) 141-150.
31. E. Kowsari, S.Y. Arman, M.H. Shahini, H. Zandi, A. Ehsani, R. Naderi, A. PourghasemiHanza and M. Mehdipour, *Corros. Sci.,* 112 (2016) 73-85.
32. M.T. Majd, M. Ramezanzadeh, B. Ramezanzadeh and G. Bahlakeh, *J. Hazard. Mater.,* 382 (2020) 121029.
33. B. Tan, S. Zhang, Y. Qiang, L. Feng, C. Liao, Y. Xu and S. Chen, *J. Mol. Liq.,* 248 (2017) 902-910.
34. D. Daoud, T. Douadi, S. Issaadi and S. Chafaa, *Corros. Sci.,* 79 (2014) 50-58.
35. S. Deng, X. Li and H. Fu, *Corros. Sci.*, 53(11) (2011) 3596-3602.
36. B. Tan, S. Zhang, Y. Qiang, W. Li, H. Liu, C. Xu and S. Chen, *J. Mol. Liq.,* 286 (2019) 110891.

37. N. V. Likhanova, P. Arellanes-Lozada, O. Olivares-Xometl, I. V. Lijanova, J. Arriola-Morales, J. C. Mendoza-Hérnandez and G. Corro, *Int. J. Electrochem. Sci.*, 14(2019) 2655-2671.
38. R.G. Sundaram, G. Vengatesh and M. Sundaravadivelu, *Surf. Interf.*, 22 (2021) 100841.
39. A. Suhasaria, M. Murmu, S. Satpati, P. Banerjee and D. Sukul, *J. Mol. Liq.,* 313 (2020) 113537.
40. S. Mo, H.Q. Luo and N.B. Li, *J. Colloid Interf. Sci.,* 505 (2017) 929-939.
41. Y. Ma, B. Fan, H. Liu, G. Fan, H. Hao and B. Yang, *Appl. Surf. Sci.*, 514 (2020) 146086
42. Y. Qiang, S. Zhang, S. Xu, L. Guo, N. Chen and Ime B. Obot, *Int. J. Electrochem. Sci.*, 11 (2016) 3147-3163.
43. Y. Qiang, S. Zhang, S. Xu and W. Li, *J. Colloid Interf. Sci.*, 472 (2016) 52-59.
44. Y. Qiang, S. Zhang and L. Wang, *Appl. Surf. Sci.,* 492 (2019) 228-238.